SCIENCE CHINA
Earth Sciences

•RESEARCH PAPER•

February 2022 Vol.65 No.2: 317–336
https://doi.org/10.1007/s11430-021-9822-y

A daily drought index based on evapotranspiration and its application in regional drought analyses

Xia ZHANG[1,2], Yawen DUAN[1*], Jianping DUAN[1], Dongnan JIAN[1,2] & Zhuguo MA[1,2]

[1] *Key Laboratory of Regional Climate-Environment Research for Temperate East Asia, Institute of Atmospheric Physics, Chinese Academy of Sciences, Beijing 100029, China;*
[2] *University of Chinese Academy of Sciences, Beijing 100049, China*

Received January 27, 2021; revised July 17, 2021; accepted July 27, 2021; published online December 2, 2021

Abstract With climate warming, frequent drought events have occurred in recent decades, causing huge losses to industrial and agricultural production, and affecting people's daily lives. The monitoring and forecasting of drought events has drawn increasing attention. However, compared with the various monthly drought indices and their wide application in drought research, daily drought indices, which would be much more suitable for drought monitoring and forecasting, are still scarce. The development of a daily drought index would improve the accuracy of drought monitoring and forecasting, and facilitate the evaluation of existing indices. In this study, we constructed a new daily drought index, the daily evapotranspiration deficit index (DEDI), based on actual and potential evapotranspiration data from the high-resolution ERA5 reanalysis dataset of the European Center for Medium-Range Weather Forecasts. This new index was then applied to analyze the spatial and temporal evolution characteristics of four drought events that occurred in southwest, north, northeast, and eastern northwest China in the spring and summer of 2019. Comparisons with the operationally used Meteorological Drought Composite Index and another commonly used index, the Standardized Precipitation Evapotranspiration Index, indicated that DEDI characterized the spatiotemporal evolution of the four drought events reasonably well and was superior in depicting the onset and cessation of the drought events, as well as multiple drought intensity peaks. Additionally, DEDI considers land surface conditions, such as vegetation coverage, which enables its potential application not only for meteorological purposes but also for agricultural drought warning and monitoring.

Keywords Actual evapotranspiration, Potential evapotranspiration, Daily drought index, Meteorological drought, Drought events

Citation: Zhang X, Duan Y, Duan J, Jian D, Ma Z. 2022. A daily drought index based on evapotranspiration and its application in regional drought analyses. Science China Earth Sciences, 65(2): 317–336, https://doi.org/10.1007/s11430-021-9822-y

1. Introduction

Drought is the most frequent and complicated meteorological disaster worldwide (Ma and Fu, 2007). In China, drought accounts for 50% of the area affected by meteorological disasters, while floods account for only 27.8% (Zhang, 2008). Drought, as the most serious meteorological disaster in China (State Scientific and Technological Commission, 1990), has caused huge losses to industrial, agricultural, and routine activities. From 2004 to 2015, the direct economic losses caused by drought exceeded an average of 64 billion Yuan per year (Liao and Zhang, 2017). In recent years, ecological environmental deterioration, such as desertification aggravation and water shortages, caused by frequent regional extreme drought events under climate warming, and their associated impacts on social and economic development, have aroused wide public concern (Lucht et al., 2002; Dai, 2013; Vicente-Serrano et al., 2013;

* Corresponding author (email: duanyw@tea.ac.cn)

© Science China Press and Springer-Verlag GmbH Germany, part of Springer Nature 2021

https://engine.scichina.com/doi/10.1007/s11430-021-9822-y

Ding and Gao, 2020).

Drought indices are important indicators for quantifying and assessing dry and wet conditions and their effects on agriculture and hydrology (Vicente-Serrano et al., 2013; Yang et al., 2017). Because of the complexity of the onset and cessation times, influence range, and intensity evolution of drought events, various drought indices have been developed to enhance the accurate description of actual dry and wet conditions. The self-calibrated Palmer Drought Severity Index (scPDSI) has been widely applied in drought research because it considers the influences of multiple factors, such as temperature. However, the difficulty in obtaining the data necessary to calculate all the parameters, the complexity of the calculation, and the timescale (9–12 months) of its application (Wells et al., 2004; Dai, 2011a), make it difficult for scPDSI to be universally applied in drought monitoring and forecasting. The Standardized Precipitation Index (SPI) has a simpler calculation method than scPDSI and can reflect the multi-scalar characteristics of drought processes. Nevertheless, as SPI is only based on precipitation, it cannot faithfully reflect the impact of temperature variability and changes on drought under the current warming conditions (McKee et al., 1993; McRoberts and Nielsen-Gammon, 2012). Therefore, it has certain limitations in practical drought research. The Standardized Precipitation Evapotranspiration Index (SPEI) uses the difference between precipitation and potential evapotranspiration (PET) to replace the precipitation anomaly in SPI, thereby combining the sensitivity of scPDSI to changes in temperature and the multi-scalar nature of SPI (Vicente-Serrano et al., 2010, 2012; Wang and Chen, 2014). However, SPEI may not accurately reflect the relationship between vegetation ecosystems and climatic dry and wet variations, because it does not fully consider land surface conditions (Mao et al., 2011; Vicente-Serrano et al., 2013; Zhang et al., 2019). Anderson et al. (2011) emphasized the importance of considering both PET and actual evapotranspiration (AET) in the construction of a drought index and proposed an evaporative stress index based on the ratio between remotely sensed AET and PET. However, this index is primarily utilized for describing drought conditions on a monthly timescale. Moreover, the applicability of a drought index based on this evapotranspiration ratio to shorter timescales (e.g., daily) is greatly limited because PET=0 is common in most regions of the world during winter (Vicente-Serrano et al., 2010).

Generally, different drought indices are constructed according to specific research perspectives or purposes and can be used in practical applications to characterize different drought intensities and their associated impacts on agriculture, water resources, and fire risk (Table 1; cited from Svoboda et al. (2002)). However, each drought index has both advantages and disadvantages. It is difficult to construct a unified index that comprehensively and fully describes all drought information and meets the needs of various users (Heim Jr., 2002; Mao et al., 2011; Yang et al., 2017). In particular, most of the drought indices that are currently used are appropriate for the detection and assessment of dry and wet conditions on timescales of months or years, while drought indices with shorter timescales (e.g., daily), which are better suited to drought monitoring and forecasting, are relatively scarce. With the rapidly increasing concurrence of abnormally high temperatures and droughts owing to a warming climate (Hao et al., 2013; Ren et al., 2020), flash droughts frequently occur (Wang and Yuan, 2018; Yuan et al., 2020). Such droughts may be of short duration (e.g., a few days or weeks), but can greatly threaten water supply (Dai, 2011b; Zhang et al., 2020) and cause significant reductions in crop yields, especially during critical plant growth stages, such as germination, pollination, and grain filling (Meyer et al., 1993; Calviño et al., 2003; Hunt et al., 2014). Currently, the widely used drought indices with timescales of months or longer have weak applicability for characterizing short-term droughts, whereas drought indices with daily timescale can more accurately describe the onset, cessation, and evolution of drought events (Couturier et al., 2001; Jia and Zhang, 2018; Li et al., 2021). Therefore, under

Table 1 The categories of drought magnitude, determined by a percentile approach, and their associated impacts on agriculture, water, and fire risk[a)]

Drought category	Percentile chance k (%)	Potential impacts on agriculture, water, and fire risk
Extreme drought	$k\leq 2$	Major, widespread crop losses; widespread water shortages and restrictions; extreme fire risk
Severe drought	$2<k\leq 10$	Crop losses likely; water shortages, restrictions imposed; fire risk very high
Moderate drought	$10<k\leq 20$	Some damage to crops; streamflow, reservoir, and well levels reduced, some water shortages; fire risk high
Abnormal drought	$20<k\leq 30$	Farm activities and crop growth slowed; streamflow below average; fire risk above average

a) Svoboda et al. (2002).

https://engine.scichina.com/doi/10.1007/s11430-021-9822-y

a changing climate, it is necessary to supplement and develop drought indices at a daily timescale. In China, a daily updated Meteorological Drought Composite Index (MCI) has been applied to monitor the real-time nationwide drought status. MCI is a complex drought index based on SPI and the relative humidity index, with a timescale of 1–5 months. By considering relatively comprehensive influencing factors, MCI can better represent the synthetic effects of drought processes (Liao and Zhang, 2017; Han et al., 2019). However, as it contains many variables, the calculation of MCI is complicated. Additionally, Wang et al. (2015) pointed out that, owing to the consideration of an excessively long period of early impact, MCI detects longer drought durations and stronger drought intensities during the mitigation stage than the actual situation entails. Therefore, to supplement or evaluate the daily MCI and improve operational drought monitoring and forecasting in China, the development of a daily drought index that can effectively characterize drought is urgently needed.

PET represents the capability of the atmosphere to obtain water vapor from terrestrial precipitation, soil moisture, runoff, water stores, and lake water, and plays an important role in regulating the water deficit that causes drought (Vicente-Serrano et al., 2012; McEvoy et al., 2016). In the context of climate warming, the increase in PET plays an important role in aggravating global aridity (Ma and Fu, 2007; Dai, 2011b, 2013; Scheff and Frierson, 2014). Many drought indices that are widely used in current meteorological drought monitoring operations and research consider PET (e.g., scPDSI, SPEI, and MCI). Many studies have shown that drought indices that consider PET are superior to those that only consider precipitation (e.g., SPI), as they can more accurately characterize drought events (Vicente-Serrano et al., 2010, 2015; Yang et al., 2017). Nonetheless, PET does not directly depend on actual land water storage, while AET represents the atmospheric water content that evaporates from water, soil, and vegetation surfaces and transpires from vegetation. Therefore, considering both PET and AET in the drought index is expected to enable better quantification of surface dryness and wetness, and their impacts on the terrestrial ecological environment (Anderson et al., 2011). Zhang et al. (2019) built a monthly drought index based on AET and PET and demonstrated that drought indices that consider both AET and PET can more reasonably detect changes in climatic dryness and wetness, and particularly, can more sensitively capture the responses of ecosystems to drought evolution.

As such, the combination of AET and PET clearly has rich physical significance, not only because it takes the maximum atmospheric demand for water and actual land water storage into account, but also because it is closely related to the ecosystem. Thus, this study attempts to construct a daily drought index based on AET and PET, and to evaluate its potential in drought monitoring and forecasting by comparing it with other daily drought indices.

Against a background of climate warming, the frequent occurrence of drought events, particularly in the north, northeast, southwest, and eastern northwest regions of China (Ma and Fu, 2001; Huang and Zhou, 2002; Huang et al., 2012), has caused huge economic losses. The prolonged extreme drought event that occurred over Yunnan Province in the southwest region in the spring and summer of 2019 caused a direct economic loss of 6562 million Yuan, exceeding the total direct economic loss caused by droughts during the previous five years (Ding and Gao, 2020). In the spring and summer of 2019, heavy regional drought events also occurred in north China, northeast China, and eastern northwest China. Based on our newly established daily evapotranspiration deficit index (DEDI), this study analyzed the temporal and spatial evolution of these four drought events with varying intensities. Furthermore, comparisons with MCI and SPEI were conducted to evaluate the potential of DEDI for use in drought monitoring.

2. Index definitions, data, and methodology

2.1 Definitions of the new drought index

In this study, a new drought index with a daily timescale is defined, based on the difference between AET and PET. It is called the daily evapotranspiration deficit index (DEDI). The formula is as follows:

$$\mathrm{DEDI}_i = \frac{D_i - D_{\mathrm{AVE}}}{D_{\mathrm{STU}}},\ D_i = \mathrm{AET}_i - \mathrm{PET}_i, \tag{1}$$

where i indicates the time, AET_i denotes the AET on day i (mm d^{-1}), PET_i denotes the PET on day i (mm d^{-1}), D_i represents the evapotranspiration deficit between AET and PET on day i, and D_{AVE} and D_{STU} are the multi-year climatic mean and standard deviation, respectively.

2.2 MCI and SPEI

MCI is a daily drought index developed by the National Climate Center and is currently used for daily updated operational drought monitoring across China (Liao and Zhang, 2017; Han et al., 2019). The formula for MCI is as follows:

$$\mathrm{MCI} = K_a\left(a\mathrm{SPIW}_{60} + b\mathrm{MI}_{30} + c\mathrm{SPI}_{90} + d\mathrm{SPI}_{150}\right), \tag{2}$$

where SPIW_{60} is the standardized weighted precipitation index for the past 60 days; MI_{30} is the relative humidity index (i.e., the ratio of the difference between precipitation and PET to PET) in the past 30 days; SPI_{90} and SPI_{150} represent the SPI in the past 90 and 150 days, respectively; a, b, c, and d are weighting coefficients, and their values vary with region and season; and K_a denotes the seasonal adjustment coefficient, which is determined according to the sensitivity

https://engine.scichina.com/doi/10.1007/s11430-021-9822-y

of the growth changes of the dominant crops in different regions and seasons to soil moisture. The detailed calculation of each component in MCI and the value of each weight coefficient can be found in the national standard "Grades of meteorological drought" (General Administration of Quality Supvision, 2017). The dry and wet classifications of MCI are shown in Table 2.

SPEI, proposed by Vicente-Serrano et al. (2010), can also be applied to a daily timescale using the following formula:

$$D_n^k = \sum_{i=0}^{k-1}(P_{n-i} - \mathrm{PET}_{n-i}), \quad (3)$$

where k is the timescale (day or month), n and i represent certain days (or months), P is precipitation, and D_n^k represents the difference between precipitation and PET on the nth day (or month) when the timescale is k. For example, when k=5, the D_n^k of the nth day (or month) equals the sum of the difference between precipitation and PET for the antecedent four days (or months) and the current day (or month). At a given timescale, SPEI was calculated by fitting the accumulated difference between precipitation and PET to a certain probability distribution, and then transforming the cumulative distribution into standard normal distribution. In this study, the Pearson-III distribution was used to fit the cumulative sequences. Pearson-III was recommended by Guttman (1999) as a universal model for calculating probability distributions. Wang et al. (2019) compared SPEI results fitted using Pearson-III, general logistic, generalized extreme value, and normal probability distributions, and demonstrated that Pearson-III fits the SPEI data in China well. The dry and wet classifications of SPEI are displayed in Table 2.

2.3 Data

To calculate DEDI in this study, we adopted 0.25°×0.25° gridded daily AET and PET data for the period 1979–2019 from the ERA5 reanalysis provided by the European Center for Medium-Range Weather Forecasts. ERA5 characterizes the surface heat budget quite accurately through a relatively good representation of surface processes and the adoption of high-quality near-surface meteorological data (Martens et al., 2020). Sun et al. (2020) investigated land-atmosphere coupling over the Tibetan Plateau in the rainy season and demonstrated that ERA5 behaves similarly to site observations. In addition, Huang et al. (2020) showed that ERA5 could reasonably describe the rules governing changes in the water cycle of the Yellow River basin under global warming, and accurately depict the increasing evapotranspiration trend in the upper reaches over the past 40 years. Su et al. (2020) also showed that ERA5 could accurately depict the spatio-temporal evolution and regional differences of the water cycle in China and major river basins under climate change. These results verify the accuracy and applicability of ERA5 data in China.

Daily MCI data for 2019, covering more than 2000 sites in China, were provided by the National Climate Center of the China Meteorological Administration (https://cmdp.ncc-cma.net/extreme/dust.php?product=dust_moni). Our study regions in southwest, north, northeast, and eastern northwest China contained 251, 619, 165, and 137 MCI stations, respectively. To allow comparisons between different datasets, we adopted Cressman interpolation to interpolate the MCI site observations to fill the 0.25°×0.25° grid.

The daily SPEI data analyzed in this study were calculated based on observational precipitation and PET data. Precipitation data were obtained from the National Meteorological Information Center of the China Meteorological Administration (http://data.cma.cn/), and PET was calculated based on the Penman-Monteith model (Allen et al., 1998), using daily observational 10-m wind speed, maximum temperature, minimum temperature, relative humidity, air pressure, and sunshine duration data from 715 sites on the website. Our study regions in southwest, north, northeast, and eastern northwest China contained 67, 112, 83, and 48 SPEI stations, respectively. The calculated SPEI

Table 2 Dry and wet classifications for the Daily Evapotranspiration Deficit Index (DEDI) in different regions in China, the Standardized Precipitation Evapotranspiration Index (SPEI), and the Meteorological Drought Composite Index (MCI)

Classification	Percentile chance k (%)	DEDI				SPEI/MCI
		Southwest	North	Northeast	Eastern northwest	
Extreme drought	k≤2	≤1.94	≤1.83	≤1.91	≤1.93	≤2.00
Severe drought	2<k≤10	−1.94–−1.30	−1.83–−1.19	−1.91–−1.19	−1.93–−1.27	−2.00–−1.50
Moderate drought	10<k≤20	−1.30–−0.93	−1.19–−0.85	−1.19–−0.83	−1.27–−0.91	−1.50–−1.00
Abnormal drought	20<k≤30	−0.93–−0.64	−0.85–−0.61	−0.83–−0.58	−0.91–−0.63	−1.00–−0.50
Normal	30<k<70	−0.64–0.50	−0.61–0.35	−0.58–0.40	−0.63–0.50	−0.50–0.50
Abnormally wet	70≤k≤80	0.50–0.86	0.35–0.75	0.40–0.76	0.50–0.86	0.50–1.00
Moderately wet	80≤k<90	0.86–1.31	0.75–1.37	0.76–1.31	0.86–1.34	1.00–1.50
Severely wet	90≤k<98	1.31–2.04	1.37–2.37	1.31–2.35	1.34–2.10	1.50–2.00
Extremely wet	k≥98	≥2.04	≥2.37	≥2.35	≥2.10	≥2.00

https://engine.scichina.com/doi/10.1007/s11430-021-9822-y

site data were not interpolated into the grid space, considering the relatively small number of available stations in each region.

2.4 Methods

(1) Penman-Monteith model used to calculate PET. The Penman-Monteith model can reasonably calculate PET under different climatic conditions and has been recommended by the Food and Agriculture Organization of the United Nations as a standard method for calculating PET (Allen et al., 1998). The formula is as follows:

$$\mathrm{PET}=\frac{0.408\Delta(R_n-G)+\gamma\frac{900}{273+T}u_2(e_s-e_a)}{\Delta+\gamma(1+0.34u_2)}, \quad (4)$$

where R_n is the net radiation (MJ m^{-2} d^{-1}), G is the soil heat flux (MJ m^{-2} d^{-1}), T is the mean air temperature (°C), u_2 is the 2-m wind speed (m s^{-1}), e_s is the saturation vapor pressure (kPa), e_a is the actual vapor pressure (kPa), (e_s−e_a) is the saturation vapor pressure difference, Δ represents the slope of the saturation vapor pressure curve (kPa °C^{-1}), and γ is the psychrometric constant (kPa °C^{-1}). Detailed calculations of each parameter in the formula are provided by Allen et al. (1998). Regular observations at meteorological stations, including maximum temperature, minimum temperature, relative humidity, 10-m wind speed, sunshine duration, latitude, and altitude, were utilized to calculate PET. The PET data from ERA5 were also calculated using the Penman-Monteith model (Hersbach et al., 2020).

(2) Standardization of DEDI. Using daily ERA5 data from 1979 to 2019, we first calculated the difference between AET and PET at each grid point. Then, the climatic average and standard deviation, derived from daily evapotranspiration difference data from 1979 to 2008, were utilized to standardize the daily evapotranspiration difference in the study year (2019), according to eq. (1), and the DEDI data needed for this study were obtained. The choice of the period used to calculate the climatology of the evapotranspiration difference was tested and was shown to have little effect on the results. Figure 1 shows that the discrepancies in the climatic values of evapotranspiration difference between the full period (1979–2019) and every 30 years from 1979 onwards are negligible. The DEDI values standardized using different climatic values of evapotranspiration difference vary little, with an average relative deviation of only 4.65%. Therefore, the first period (1979–2008) of evapotranspiration difference was chosen as the climatic value to standardize the evapotranspiration difference. This approach made the calculation more convenient and would benefit the instant calculation of DEDI values in real-time drought monitoring and forecasting using the latest released data.

(3) Dry and wet DEDI classifications. In this study, a percentile threshold method (Svoboda et al., 2002; Hobbins et al., 2004) was used to classify the DEDI dryness and wetness and determine the intensity of drought. Using daily DEDI from 1979–2019, the abnormal, moderate, severe, and extreme drought thresholds were confined to 21–30%, 11–20%, 3–10%, and ≤2%, respectively (Table 2). The dry and wet classifications for each of our study regions (southwest, north, northeast, and eastern northwest China) were divided separately using the percentile threshold method, considering regional differences. As shown in Table 2, the drought classification determined by this percentile approach is convenient for matching and comparison with other indicators. For instance, the drought magnitude of scPDSI, SPEI, and SPI can also be classified using percentile thresholds (Svoboda et al., 2002).

(4) Calculation of the drought coverage percentage. In this study, the percentage of drought coverage was used to analyze temporal variation in spatial drought condition during drought events with different intensities (Zou et al., 2010). For the grid and station data, the formulas are as

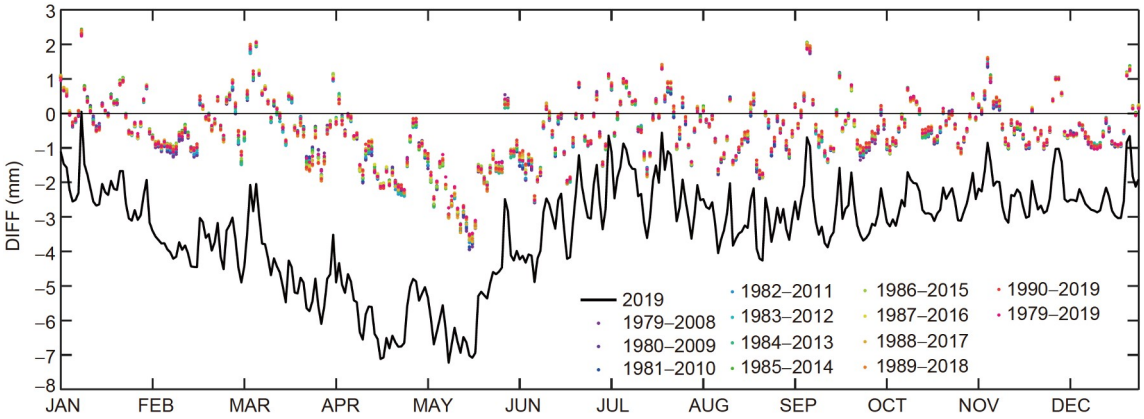

Figure 1 Intra-annual variations of daily evapotranspiration difference averaged over the southwest China region (21°–30°N, 97°–107°E). DIFF represents the difference between actual evapotranspiration and potential evapotranspiration; the black line shows the daily variations of evapotranspiration difference in 2019; the colored dots denote the daily deviations of evapotranspiration difference in the year 2019 from those in different periods from 1979 to 2019.

https://engine.scichina.com/doi/10.1007/s11430-021-9822-y

follows:

$$S_{i,c}=\begin{cases}\dfrac{x_{i,c}\times y_{i,c}}{x_0\times y_0}\times 100\%,\\ \dfrac{N_{i,c}}{N_0}\times 100\%,\end{cases} \tag{5}$$

where c represents different drought categories (nine categories can be seen in Table 2); i denotes the time; $x_{i,c}$ and $y_{i,c}$ represent the number of grid points for longitude and latitude, respectively, occupied by the c drought category on the ith day; x_0 and y_0 represent the sum of the grid points in the study region for longitude and latitude, respectively; $N_{i,c}$ indicates the number of stations occupied by the c drought category on the ith day, and N_0 indicates the sum of all stations in the study region.

3. Results

3.1 Drought signals of the 2019 southwest China drought event identified by DEDI

To clearly understand the temporal and spatial characteristics of drought events, we first analyzed the spatial evolution of daily drought conditions. The entire drought process from occurrence to relief lasted approximately 180 days; thus, as it was unrealistic to place so many daily spatial figures in the main text, the daily drought evolutions detected by DEDI are displayed as dynamic pictures in the attachments, while the half-monthly DEDI averages are shown in the main text. As shown in Appendix Figure S1 online (https://link.springer.com), the southwest region (21°–30°N, 97°–107°E) experienced heavy drought in the spring and summer of 2019, especially in Yunnan Province. Furthermore, the half-monthly DEDI averages (Figure 2) show that the drought began in late March over central Yunnan, the intensity then increased rapidly in late April and the extent expanded to most parts of Yunnan Province, northern Sichuan Province, and western Guizhou Province. The Red River basin in Yunnan Province exhibited particularly extreme drought. In May, the drought intensity in Yunnan Province continued to increase, and the range of droughts classified as severe and above extended in a northwesterly direction from the Red River basin in Yunnan to the Xishuangbanna and Pu'er municipalities. The drought eased slightly in June; subsequently, most parts of the southwest displayed normal or humid conditions in July. A second peak of drought appeared in August, and the drought-affected area covered almost the entire southwest region, but the peak lasted only a short period, and the region finally returned to normal by the beginning of September.

To evaluate the ability of the newly constructed DEDI to represent the temporal and spatial evolution of this extreme drought event, the MCI and SPEI analyses are presented in Figures 3 and 4. From the MCI analysis in Figure 3, a slight drought began to develop over Yunnan Province in early April, then intensified to an extreme drought over central and western Yunnan in May. Almost the entire Yunnan area exhibited a state of extreme drought until June. The drought intensity began to weaken and the drought range to narrow in July, but most parts of Yunnan Province persistently presented relatively mild drought conditions from August to September. Unlike MCI, SPEI (Figure 4) generally presented similar drought characteristics (timing and spatial evolution) to DEDI, and the drought detected by SPEI also experienced two peaks, in May and August, respectively. However, the drought intensity detected by SPEI was slightly weaker than that detected by DEDI. The drought detected by SPEI in the Red River basin of Yunnan did not reach the extreme category in late April, and in June the drought eased over the central and western areas of Yunnan, which presented moderate drought in DEDI.

3.2 Evolution of the 2019 southwest China drought event depicted by DEDI

From the spatial patterns of the daily drought evolution characterized by DEDI (Appendix Figure S1 online), the areas with the strongest drought magnitude in the 2019 southwest extreme drought event were mainly located in the central and western parts of Yunnan Province from late April to late June. Therefore, the region (21°–26.2°N, 98.3°–103.6°E) was selected as the critical zone of the drought event (the gray dashed boxes in Figures 2–4) to further analyze the evolution of the drought process.

Figure 5 shows the daily variations of the original DEDI and its values smoothed on weekly, semi-monthly, and monthly scales from March 16 to September 15, 2019. The evolution of DEDI using various time windows reflects that the drought event experienced two stages. The drought began in late March, after persistent development from April to May, it reached a peak in May, weakened in June with alternation between dry and wet, and eased in the middle of July. The second stage of the drought event began to develop in late July and reached its peak in mid-August, presenting a relatively short duration. The humid conditions that appeared in early September quickly alleviated the drought, indicating that the end of the drought event occurred during the seasonal change from spring to summer. The DEDI 31-day moving average smoothed out dryness and wetness fluctuations at timescales shorter than a month and displayed smoother drought changes, similar to the variations displayed by MCI. The second process of the drought event monitored by DEDI in August lasted only about a month and contained several dry and wet fluctuations, therefore the drought magnitude after being smoothed was much weaker than that in the first drought stage. Unlike DEDI, MCI

https://engine.scichina.com/doi/10.1007/s11430-021-9822-y

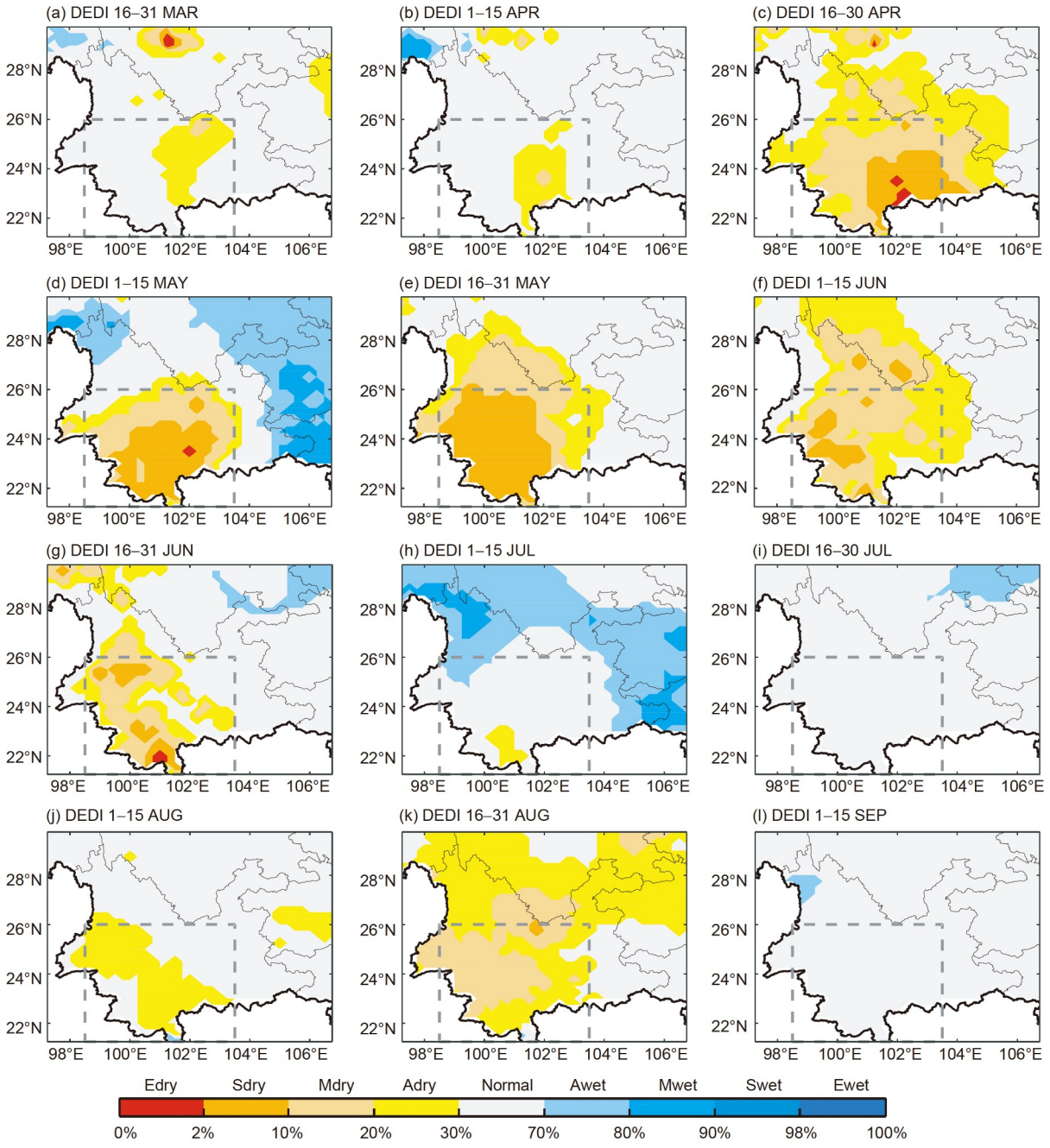

Figure 2 Spatial patterns of semi-monthly DEDI averages over southwest China from March 16 to September 15, 2019. The areas with the strongest drought in this drought event were mainly located in central and western Yunnan Province (21°–26.2°N, 98.3°–103.6°E) from late April to late June, so it was selected as the critical region (the gray dashed box) for subsequent time series analysis. Edry, extremely dry; Sdry, severely dry; Mdry, moderately dry; Adry, abnormally dry; Ewet, extremely wet; Swet, severely wet; Mwet, moderately wet; Awet, abnormally wet.

showed that the transition from wet to dry occurred in early April. After continuous strengthening until mid-June, the drought intensity began to weaken, and, despite a short wet period in late July, a slight drought state remained in the region. MCI presented a remarkable discrepancy when compared with the 31-day smoothed DEDI; the DEDI peak appeared in May, while the MCI peak lagged by one month. The drought evolution characterized by the 31-day smoothed SPEI was very consistent with that of DEDI, while the onset and peak time of the MCI-monitored drought lagged behind those of both SPEI and DEDI.

From the daily coverage percentage of moderate, severe, and extreme droughts monitored by DEDI (Figure 6), the drought area constantly expanded from April, especially the area of extreme drought, and the drought coverage reached its maximum of approximately 60% in mid-May. Compared with the climatic mean of 1979–2019, the drought in the spring and summer of 2019 presented a remarkably different

https://engine.scichina.com/doi/10.1007/s11430-021-9822-y

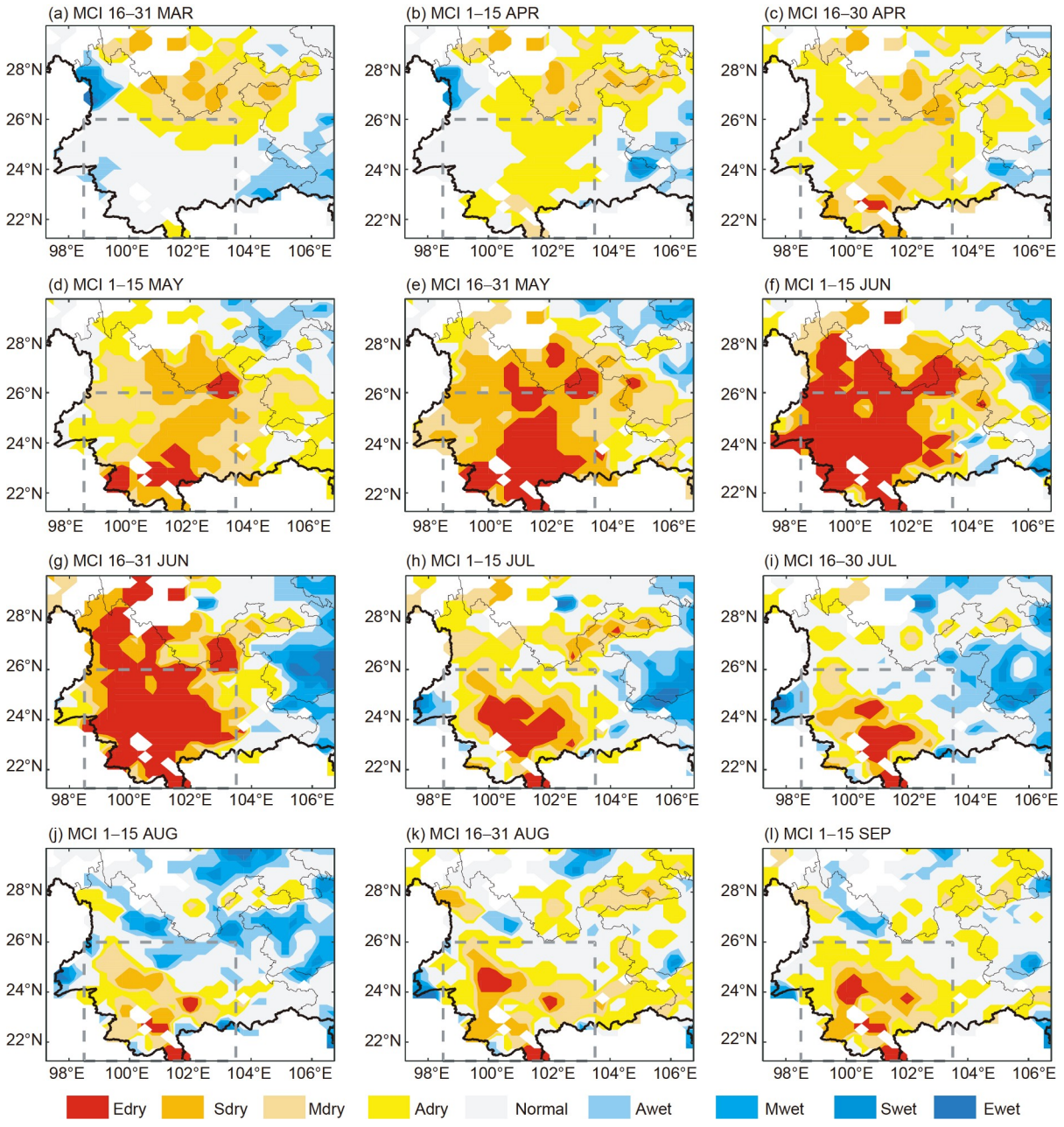

Figure 3 Spatial patterns of semi-monthly MCI averages over southwest China from March 16 to September 15, 2019. The gray dashed box indicates the critical region (21°–26.2°N, 98.3°–103.6°E) of the drought event. Edry, extremely dry; Sdry, severely dry; Mdry, moderately dry; Adry, abnormally dry; Ewet, extremely wet; Swet, severely wet; Mwet, moderately wet; Awet, abnormally wet.

seasonal evolution. In terms of the multi-year average, droughts classified as moderate and stronger developed markedly in the early spring. Drought intensity then strengthened owing to seasonal precipitation shortages and rising temperatures. Drought intensity and range were markedly reduced in late May owing to the approach of the rainy season in the southwest. In 2019, no or slight drought occurred in early spring, and the studied drought only began to develop in late March. The drought magnitude thereafter was generally much higher than the climatic average. These results indicate the long duration and severity of the drought event in 2019. The spatial coverage of the drought areas with different intensities monitored by SPEI showed temporal variations consistent with those monitored by DEDI. In contrast, MCI detected that the drought magnitude intensified into the extreme category in early May, the drought range reached a maximum of 60% in early and mid-June, and the detected peak time of the drought lagged one month relative to that of DEDI. In addition, DEDI detected that the coverage percentage of severe drought in August was generally approximately 30%, occasionally reaching as high as 50%. This indicates that the impact of the second stage of the

https://engine.scichina.com/doi/10.1007/s11430-021-9822-y

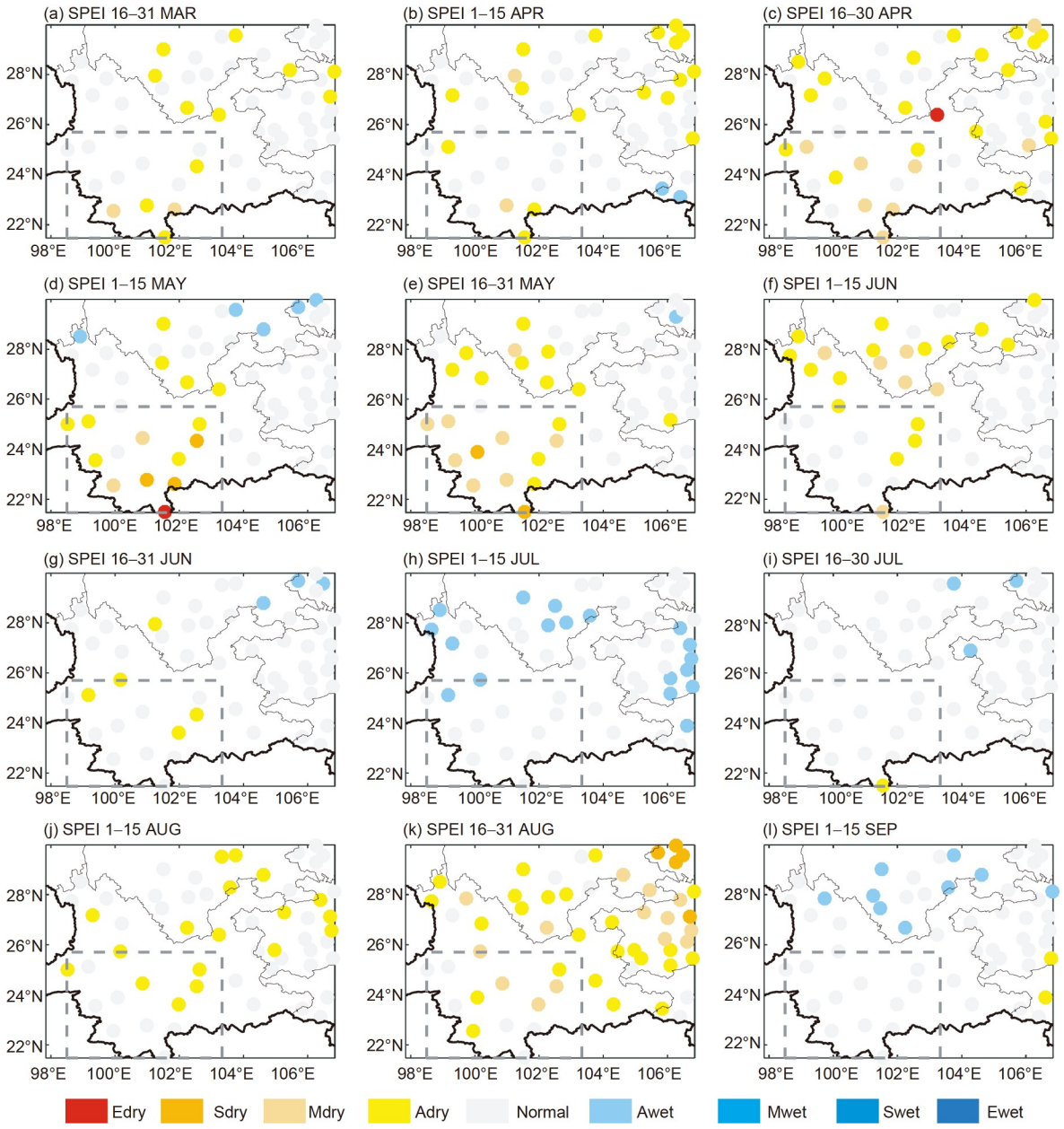

Figure 4 Spatial patterns of semi-monthly SPEI averages over southwest China from March 16 to September 15, 2019. The gray dashed box indicates the critical region (21°–26.2°N, 98.3°–103.6°E) of the drought event. Edry, extremely dry; Sdry, severely dry; Mdry, moderately dry; Adry, abnormally dry; Ewet, extremely wet; Swet, severely wet; Mwet, moderately wet; Awet, abnormally wet.

drought event should not be ignored, although it only lasted for a short period.

The above analysis shows that the drought events mainly occurred from April to August 2019. Figure 7 shows the evolution of dry and wet conditions from April to August in 1979–2019, monitored by DEDI. From the long-term time series data, DEDI detected that the drought that occurred in the spring and summer of 2019 could be regarded as a record-breaking extreme event in Yunnan, considering the last 40 years. The DEDI from 1979–2019 exhibited distinct annual variations. The region presented an apparent transition from wet to dry starting in the early 1990s, and continuous drying with a linear tendency coefficient of −0.0063 (passing the 99% confidence level). The lowest value of DEDI appeared in the year 2019. Through further analysis of annual variations in the climatic means for April to August, serious drought (with especially extreme values in May) occurred in all months except for April, which was normal and slightly dry. These results suggest the rare extremity of the drought event of 2019.

Previous studies have shown that persistently low precipitation owing to the abnormally late arrival of the rainy season and the abnormally large PET value were the main reasons for the southwest, especially Yunnan Province, to

https://engine.scichina.com/doi/10.1007/s11430-021-9822-y

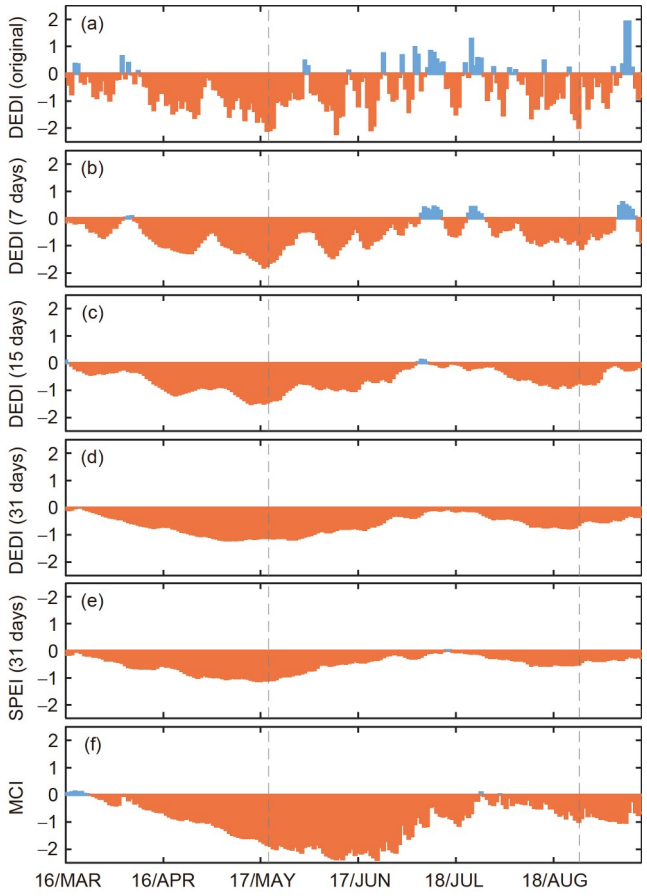

Figure 5 Daily evolutions of (a) the original DEDI values, (b)–(d) DEDI values after being smoothed over 7, 15, and 31 days, (e) the 31-day smoothed SPEI values, and (f) MCI, averaged over the typical arid region of southwest China (21°–26.2°N, 98.3°–103.6°E) from March 16 to September 15, 2019. The gray dashed lines indicate the two drought peaks detected by DEDI in May and August.

become the center, with a high incidence of drought throughout southern China (Huang and Zhou, 2002; Huang et al., 2012). Compared with the same period in previous years, the significantly stronger Australian high pressure in 2019 resulted in a weaker southern branch trough and an abnormally strong anticyclone over the Bay of Bengal. This weakened the meridional transportation of water vapor into Yunnan and led to an abnormally late rainy season in the southwest (Liu and He, 2019; Ding and Gao, 2020). However, the drought was relieved by heavy precipitation in late June, delayed by about one month compared with previous years; therefore, the lack of effective precipitation led to the rapid development of the drought in Yunnan from May to June. These results are consistent with the drought evolution characterized by the DEDI.

3.3 Performance of DEDI in characterizing the 2019 north China drought process

The daily drought evolution detected by DEDI (Appendix Figure S2 online) indicates that a heavy drought event occurred over north China in the spring of 2019. Therefore, to evaluate and examine the regional applicability of DEDI in characterizing drought signals, Figure 8 shows a comparison of the spatial evolution of the weekly averages of DEDI, MCI, and SPEI in north China (34°–42°N, 106°–120°E). The drought began to develop in late February, and a wide range of moderate drought events occurred from early March to mid-March. The drought intensity continued to deepen in late March, and extreme drought events appeared in some areas. The intensity and extent of drought started to decrease in early and mid-April, and the drought eased in late April, presenting relatively humid conditions over almost the entire area. DEDI was able to reproduce this drought process well. However, DEDI captured earlier development of the drought than MCI. DEDI indicated that slight drought occurred in Shanxi and Shandong Provinces at the end of February. The intensity then increased rapidly in the middle of March. Areas such as the Shanxi, Shandong, northern Henan, and southern Hebei Provinces presented severe drought, and areas in the northwestern Shandong and northern Henan Provinces showed extreme drought. The drought detected by SPEI was alleviated more quickly than those detected by MCI or DEDI. SPEI identified areas, including the Shanxi, Hebei, and Shandong Provinces, that were in slight drought or normal conditions at the end of March, when they still presented very serious drought conditions in MCI and DEDI.

Furthermore, the regional DEDI averages in north China were used to analyze the characteristics of the drought process. Figure 9 shows the daily evolution of DEDI, SPEI, and MCI from February 16 to April 30, 2019. Both MCI and DEDI indicated that the severity of the drought event resulted from continuous dryness from early March to mid-April, and that the drought began to ease in April. As the length of the smoothing timescale increased, DEDI presented transitions between dry and wet periods and changes in drought intensity similar to those of MCI, although the dry and wet variations monitored by MCI lagged behind those of DEDI. DEDI detected that the drought began to develop in late February, while the onset of drought in MCI was in early March, lagging one week relative to DEDI. Moreover, DEDI detected the peak drought intensity in mid-March, while the peak intensity in MCI lagged by about half a month. The drought process monitored by SPEI presented a temporal evolution similar to that of DEDI.

The drought in north China was closely related to atmospheric circulation anomalies, such as the weakening of the East Asian summer monsoon, the strengthening of the mid-latitude westerly circulation, stronger Siberian high pressure, and weaker subtropical high pressure in the central and eastern North Pacific (Zhang et al., 2003; Xu et al., 2005; Huang et al., 2006). In March, the monsoon was relatively weak, and the rain band did not move northward in China,

https://engine.scichina.com/doi/10.1007/s11430-021-9822-y

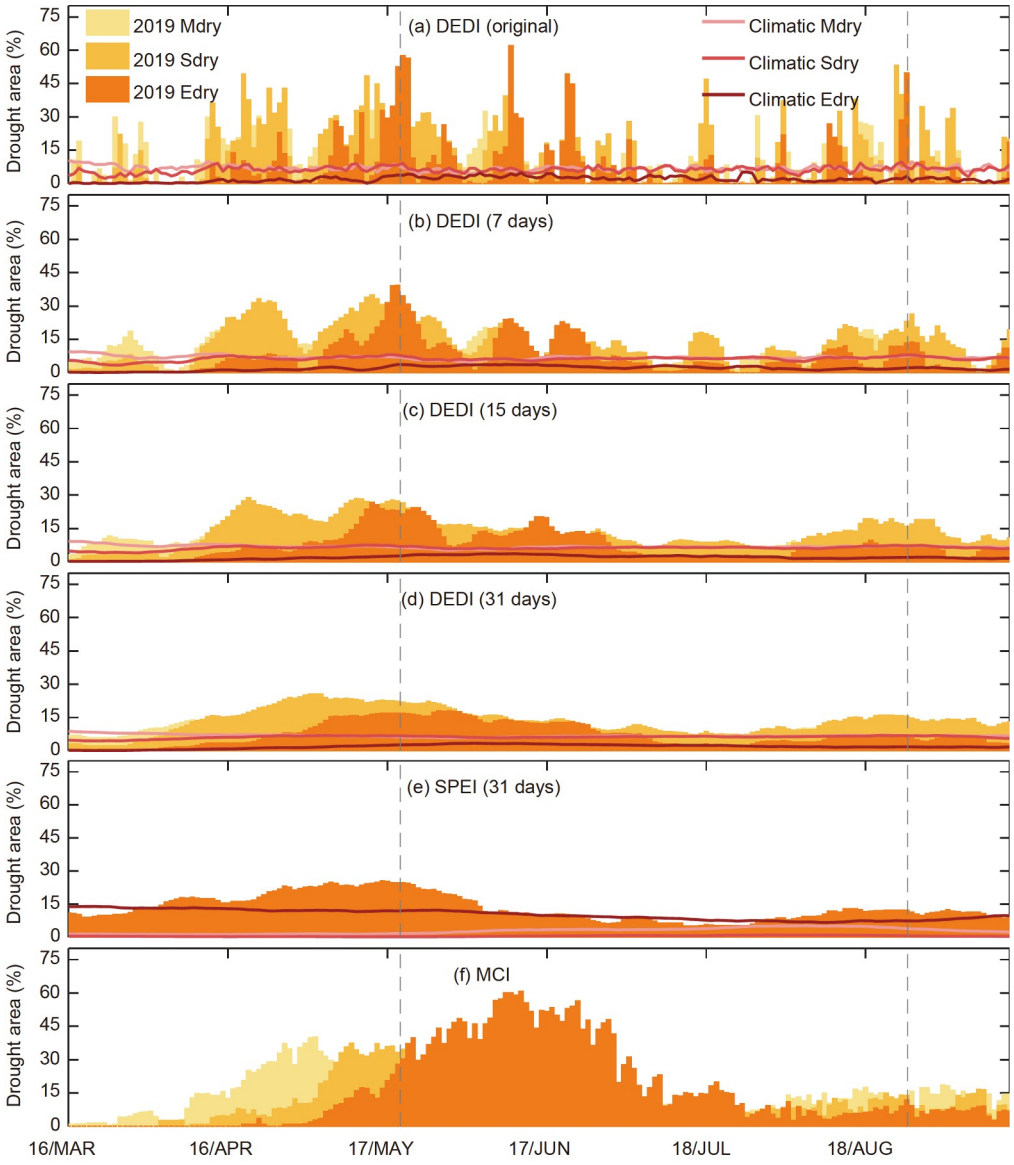

Figure 6 Daily evolutions of the drought area percentages for moderate (Mdry), severe (Sdry), and extreme (Edry) drought detected by the original DEDI and the index values after being smoothed across 7, 15, and 31 days, the 31-day smoothed SPEI values, and MCI, averaged over the typical arid region of southwest China (21°–26.2°N, 98.3°–103.6°E) from March 16 to September 15, 2019. The curve lines represent the climate mean from 1979–2019 (Note: As MCI climatological data are not available, only the climate averages of the drought areas monitored by DEDI and SPEI are displayed). The gray dashed lines indicate the two drought peaks detected by DEDI in May and August.

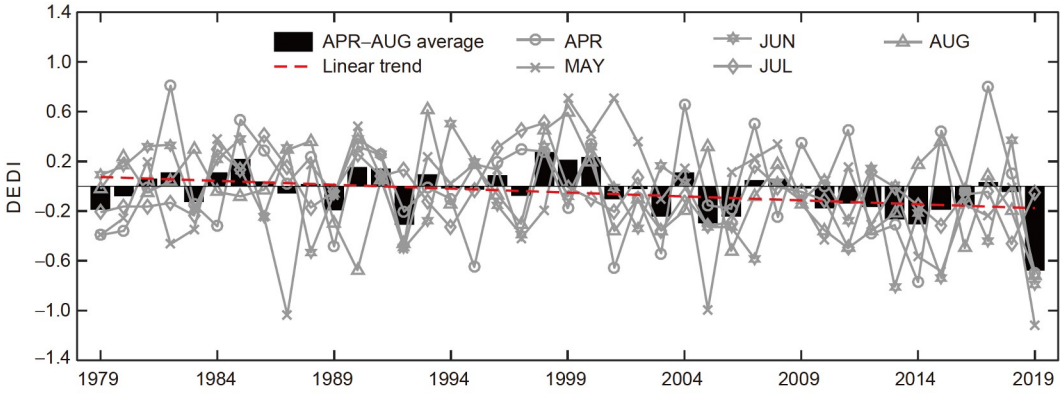

Figure 7 Annual evolutions of DEDI averaged over the typical arid region of southwest China (21°–26.2°N, 98.3°–103.6°E) from April to August 1979–2019.

https://engine.scichina.com/doi/10.1007/s11430-021-9822-y

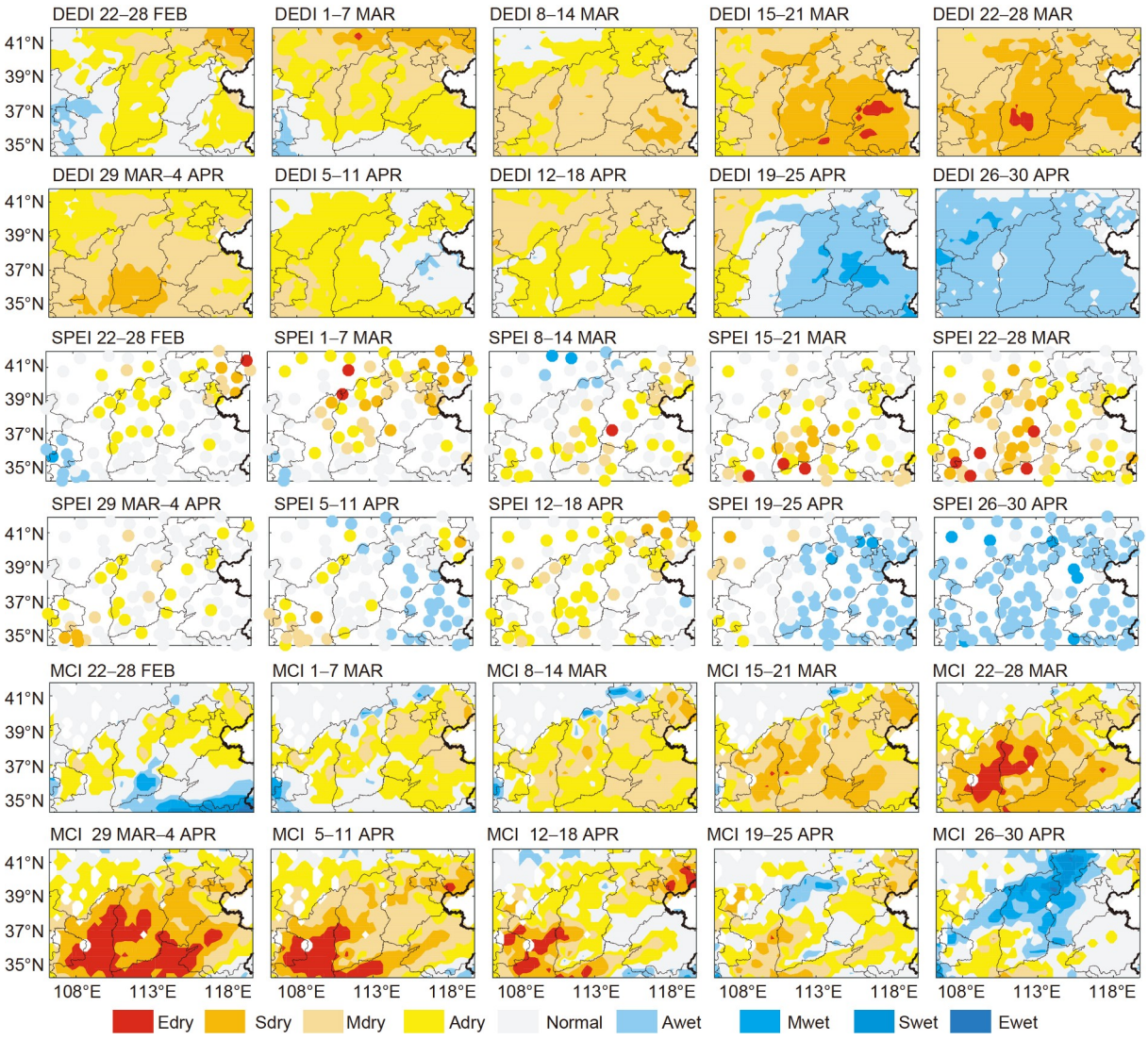

Figure 8 Spatial patterns of the weekly averages of DEDI, SPEI, and MCI over north China from February 22 to April 30, 2019. Edry, extremely dry; Sdry, severely dry; Mdry, moderately dry; Adry, abnormally dry; Ewet, extremely wet; Swet, severely wet; Mwet, moderately wet; Awet, abnormally wet.

resulting in a lack of precipitation in north China. In addition, a rapid increase in surface temperature, high evaporation, and high water consumption for spring plowing make north China prone to severe drought in spring (Huo et al., 2000; Ma et al., 2010). The drought characteristics detected by DEDI correspond well with the above processes.

3.4 Performance of DEDI in characterizing the 2019 northeast China drought process

The drought evolution shown by the daily DEDI values (Appendix Figure S3 online) indicated that the northeast region (40°–50°N, 120°–130°E) experienced a heavy drought event from April to May 2019. Figure 10 further compares the spatial evolution of the weekly averages of DEDI, MCI, and SPEI in the northeast region. The DEDI results indicated that most parts of the northeast experienced slight to moderate drought throughout April. The drought intensity increased rapidly and reached its peak from early to mid-May. Most parts of Jilin Province experienced extreme drought that lasted about a week. The drought began to ease from mid- to late May, after which most of the northeast was under normal or wet conditions. DEDI showed that slight drought began to occur in areas such as the Jilin, Heilongjiang, and Liaoning Provinces from late March, when MCI and SPEI still presented humidity or normal conditions over most areas, only displaying widespread drought conditions after about half a month. Additionally, after the initial onset of drought, DEDI and MCI indicated that the drought continued to develop from early April to early May, while the drought process monitored by SPEI was interrupted. SPEI detected that normal conditions were restored in most parts of northeast China from April 22 to April 28, and the drought developed rapidly in early May. The drought conditions in

https://engine.scichina.com/doi/10.1007/s11430-021-9822-y

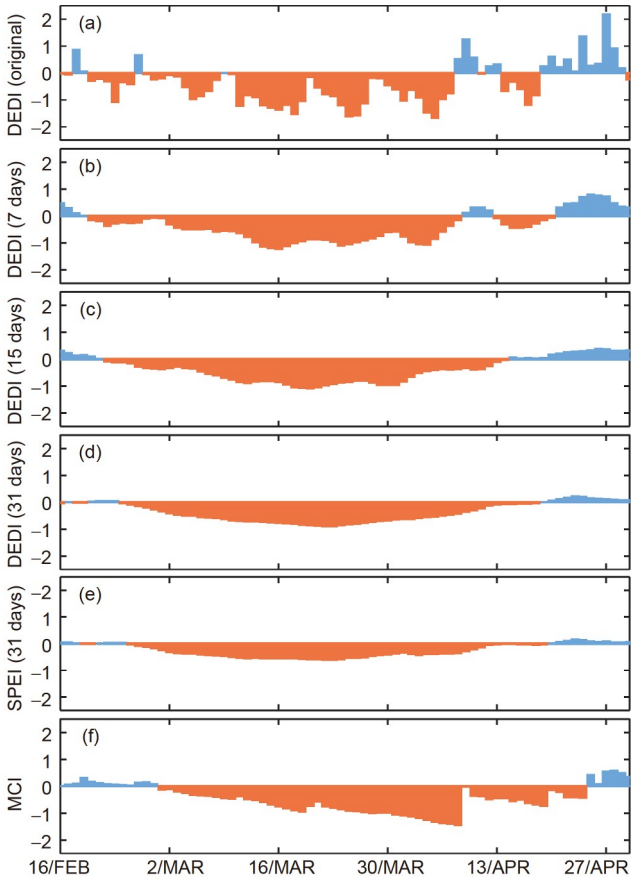

Figure 9 Daily evolutions of (a) the original DEDI values, (b)–(d) DEDI values after being smoothed over 7, 15, and 31 days, (e) the 31-day smoothed SPEI values, and (f) MCI, averaged over north China from February 16 to April 30, 2019.

most areas of Jilin Province, especially, deepened to an extreme category.

Furthermore, Figure 11 shows the daily evolutions of DEDI, SPEI, and MCI averaged across Jilin Province, where the most extreme drought occurred. DEDI detected that the drought began to develop before April, and two peaks occurred around April 15 and May 8, before the drought was relieved in late May. In contrast, MCI showed that the drought began to develop in early April. The drought intensity continued to increase, remaining persistently strong from early to mid-May, and then it weakened remarkably in late May. According to the original and 7-day smoothed DEDI values, the distinct humid state from April 22 to 28 interrupted the drought process and formed two peaks. The drought characteristics presented by DEDI were similar to those of SPEI (Figure 10), indicating that DEDI can better reveal the temporary relief of drought during periods of precipitation, while MCI may present excessive drought intensity. The SPEI values smoothed over 31 days showed a similar drought evolution to that of DEDI.

As the temperature over the northeast rose in spring, seasonal snowmelt was helpful in alleviating the drought. However, the surface evaporation increased rapidly owing to the prolonged sunshine (Ma and Fu, 2006; Tu et al., 2012), and the weak southwestern water vapor transport caused a lack of effective local precipitation (Wei and Zhang, 2009; Lu et al., 2015). In addition, the northeast region, as the largest commodity grain production region in China, experiences frequent spring plowing activities from April onwards, and both industrial and agricultural water consumption has also increased (Tu et al., 2012), leading to the aggravation of drought in the northeast from April to May. The 2019 spring northeast drought event detected by DEDI presents drought evolution characteristics corresponding with the above processes.

3.5 Performance of DEDI in characterizing the 2019 eastern northwest China drought process

The three drought events analyzed above indicate that the constructed DEDI can characterize drought events with different intensities. However, southwest, north, and northeast China are mainly located in humid and sub-humid regions of China. To more comprehensively evaluate the capabilities of DEDI in characterizing drought processes, the drought event that occurred over eastern northwest China in 2019 was selected as a typical case representing arid and semi-arid regions and is analyzed in this section.

The daily drought evolution identified by DEDI (Appendix Figure S4 online) shows that serious drought occurred in the eastern northwest from mid-March to late April 2019. Figure 12 compares the spatial characteristics of the weekly DEDI, MCI, and SPEI averages in the eastern northwest region. DEDI detected that the drought developed rapidly from north of Gansu toward the southeast in early March, and almost all of the Ningxia Hui Autonomous Region and Gansu Province were in a state of moderate drought or worse from mid-late March to mid-late April. The drought eased at the end of April, presenting normal or slightly wet conditions over most areas, except for slight drought in regions such as Maqu County in Gansu Province. In contrast, the drought development monitored by MCI and SPEI lagged somewhat. MCI showed that there was a slight draught in the Ningxia Hui Autonomous Region from early March, but drought over the northern and eastern parts of Gansu Province was not detected until the end of March. SPEI detected slight to moderate drought in the Ningxia Hui Autonomous Region and in eastern Gansu Province in late March, but normal and wet conditions covered almost the entire area by late March.

According to the spatial evolution of drought conditions indicated by the drought indices, this drought event mainly occurred in Gansu Province and the Ningxia Hui Autonomous Region, which were jointly regarded as the typical region for the subsequent time series analysis, considering that the two regions are adjacent. Figure 13 shows the daily evolution of

https://engine.scichina.com/doi/10.1007/s11430-021-9822-y

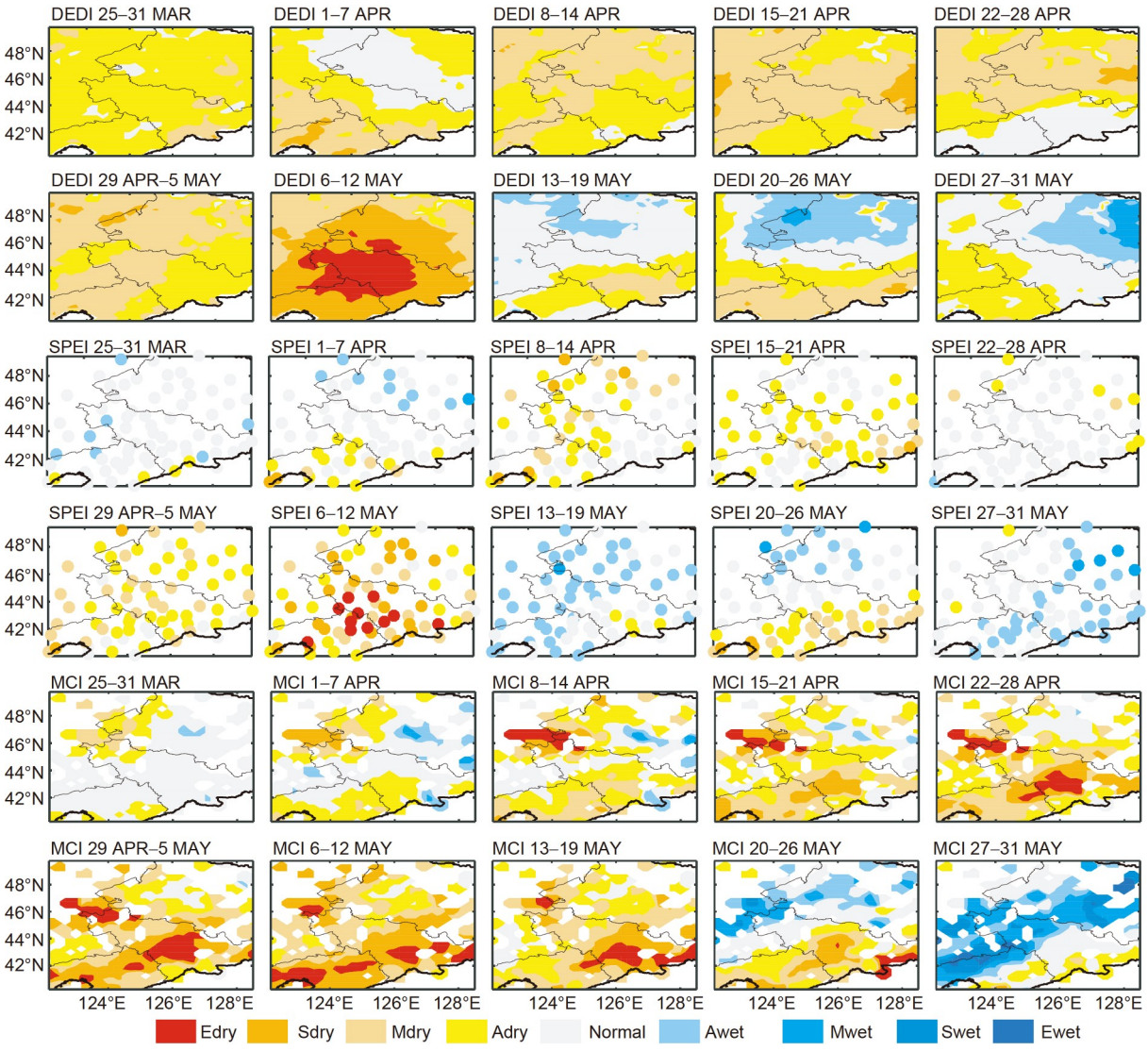

Figure 10 Spatial patterns of weekly DEDI, SPEI, and MCI averages over northeast China from March 25 to May 31, 2019. Edry, extremely dry; Sdry, severely dry; Mdry, moderately dry; Adry, abnormally dry; Ewet, extremely wet; Swet, severely wet; Mwet, moderately wet; Awet, abnormally wet.

DEDI, SPEI, and MCI in the typical region. DEDI indicated that the drought began to develop around March 5, and the intensity then gradually strengthened, reaching its peak in early April. After a short period of fluctuations between dry and wet conditions, the drought developed markedly from mid- to late April. It finally eased in late April. Comparing DEDI and SPEI smoothed over 31 days, as well as MCI, shows that the drought evolution characterized by SPEI was generally the same as that presented by DEDI; however, the drought lagged by about a week and half a month in SPEI and MCI, respectively. Moreover, the duration of the drought identified by SPEI and MCI was approximately five days shorter than that described by DEDI.

The eastern northwest region, located in the transition zone between the Tibetan Plateau and Loess Plateau, acts as a critical area for the transport of warm and humid ocean airflow into northwest inland regions. It is one of the main water shortage areas in China, with a climatic average precipitation of less than 400 mm per year (Yao, 1992; Zhang et al., 2008). A lack of precipitation and high temperatures are the main causes of drought in the eastern northwest (Ma, 2005; Ma and Shao, 2006), which makes the region prone to severe drought in spring. In the 2019 drought event, the temperature continued to rise from the beginning of spring, and the drought developed continuously from March to early April owing to weak monsoons and insufficient rainfall. Later, in mid-April, the monsoon intensified and widespread precipitation occurred in the northern Yangtze River, gradually easing the drought in this region.

4. Discussion

In this study, we evaluated the performance of one newly

https://engine.scichina.com/doi/10.1007/s11430-021-9822-y

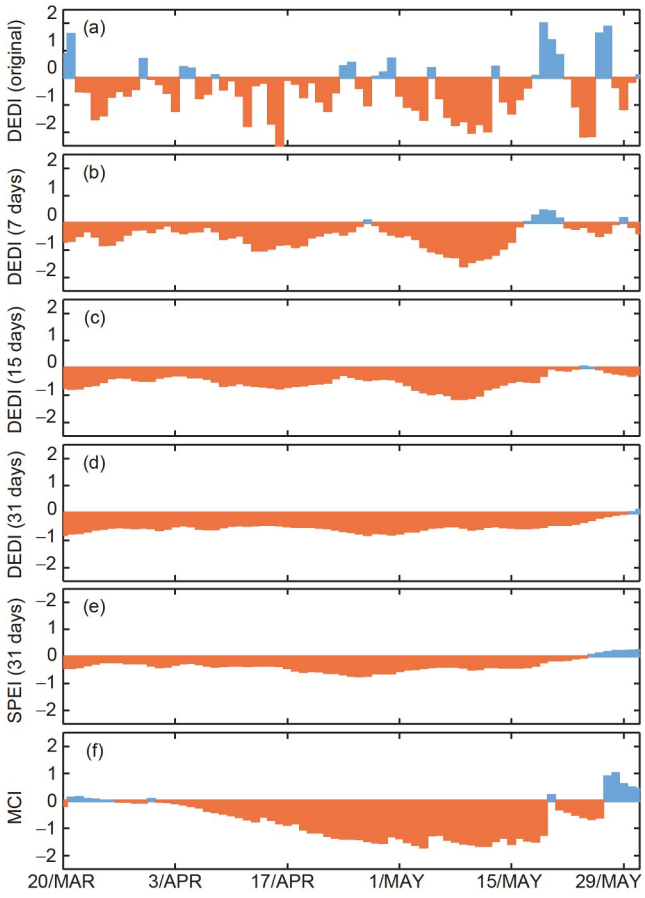

Figure 11 Daily evolutions of (a) the original DEDI values, (b)–(d) DEDI values after being smoothed over 7, 15, and 31 days, (e) the 31-day smoothed SPEI values, and (f) MCI, averaged over Jilin Province from March 20 to May 31, 2019.

defined and two currently used daily drought indices in depicting drought characteristics. Four drought events with different intensities that occurred over various dry and wet climate zones in southwest, north, northeast, and eastern northwest China in 2019 were analyzed. The results show that the ability of DEDI to identify drought features, such as the onset and cessation, spatial extent, and intensity of drought, is generally consistent with MCI and SPEI, but the details of the detected drought information varied between the drought indices. The following discusses the superiority and uncertainty of DEDI, compared to MCI and SPEI.

4.1 Superiority of DEDI over MCI and SPEI

MCI, which considers the effective precipitation and atmospheric evaporation demand accumulated over the past 1–5 months, can effectively overcome the large jumps in the index value caused by rapid increases and decreases in soil moisture (Liao and Zhang, 2017; Han et al., 2019). However, as MCI integrates the cumulative effect of recent months, it can easily overlook intense drought processes with relatively short durations. For example, Figures 2–4 show that the heavy drought events over southwest China in 2019 experienced two peak drought stages when monitored by DEDI and SPEI. The first stage of the drought occurred from April to June, reaching peak intensity in May before returning to normal or humid conditions in July. The second stage developed in early August, and the drought intensity reached its peak in late August. In contrast, the drought intensity detected by MCI varied little after the drought was relieved in early July. In practical drought monitoring and forecasting, a detailed understanding of the phased development of the drought process is helpful for relevant departments, such as agriculture and the environment, allowing them to adjust their policies promptly. In addition, by considering atmospheric conditions accumulated over the previous five months, MCI may present obvious early effects of drought events. This would result in lagging drought mitigation time, more serious drought during the mitigation period, and a longer drought duration than the actual situation (Wang et al., 2015). For example, the drought conditions in northeast China (Figure 10) detected by DEDI and SPEI weakened substantially in mid-May, and most areas returned to a normal or humid state; however, the drought conditions monitored by MCI still presented as moderate or even extreme in most areas. Similar situations also occurred over southwest China in early September (Figures 2–4) and north China in mid-April (Figure 8).

Many commonly used drought indices (including MCI and SPEI) only focus on PET, ignoring the differences in the physical mechanisms of PET and AET and the insufficient representation of PET in surface water processes (Heim Jr., 2002; Mao et al., 2011; Tu et al., 2012). According to the theoretical formula of evapotranspiration, PET is related to radiation energy, atmospheric water content, and other atmospheric state variables, which can reflect atmospheric water demand under sufficient water supply conditions. AET reflects the actual water budget and is closely related to the ecosystem through vegetation transpiration and soil evapotranspiration. DEDI, which is constructed based on AET and PET, can sensitively reflect the water budget against the background of climate warming, and considers land surface conditions such as vegetation and soil. Therefore, although DEDI contains only two parameters, it has rich physical meaning.

Finally, just as SPI and SPEI have multi-scalar characteristics, for example, the indices within 1–2 months reflect short-term drought conditions, the indices within 3–6 months reflect seasonal changes, and the indices within 12–24 months reflect inter-annual changes in drought, DEDI can also be applied to monitor drought conditions at different timescales. Because the time resolution of DEDI is daily, it can show the occurrence and development of drought day by day, avoiding the omission of short-term intense drought

https://engine.scichina.com/doi/10.1007/s11430-021-9822-y

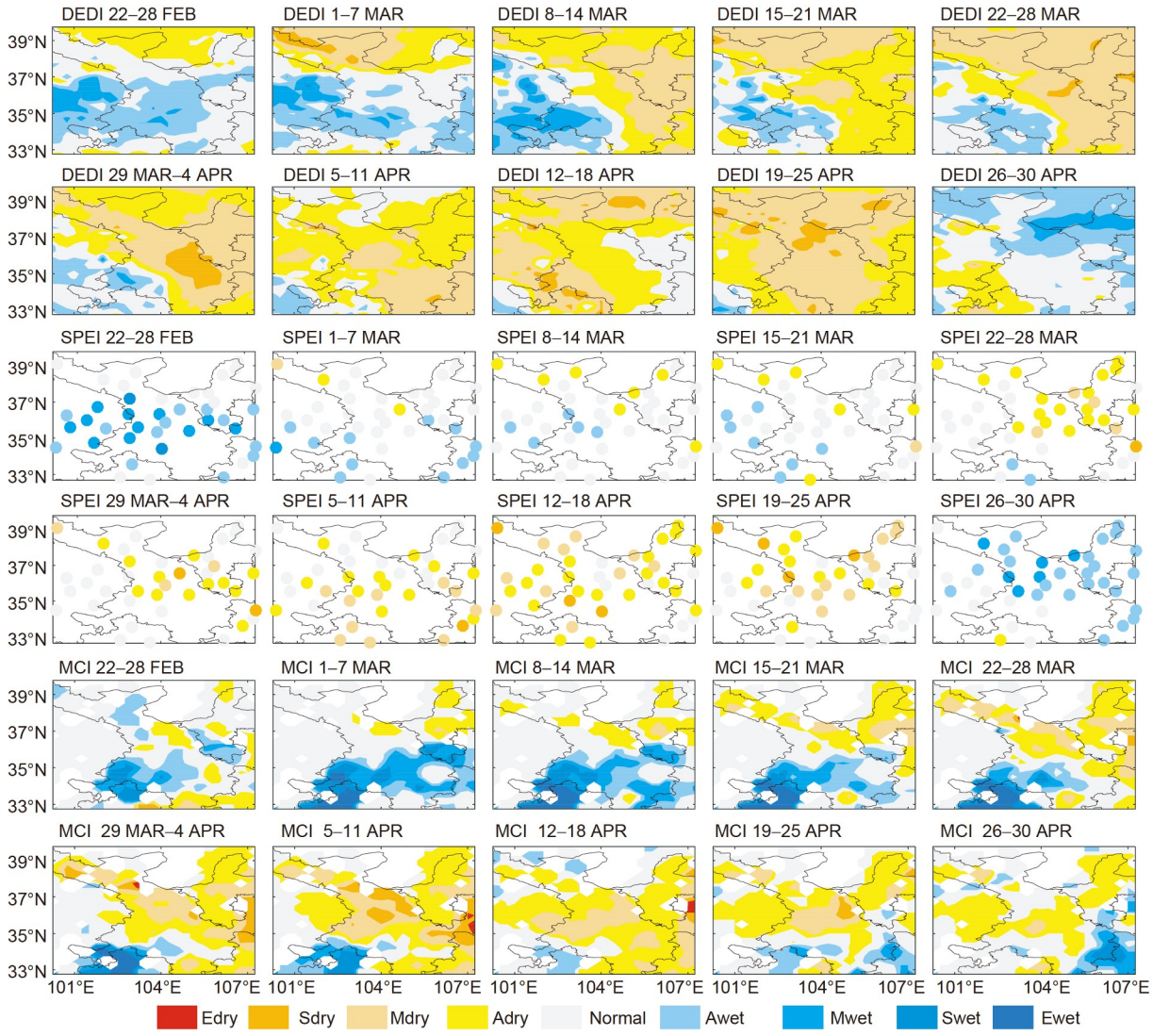

Figure 12 Spatial patterns of the weekly DEDI, SPEI, and MCI averages over eastern northwest China from February 22 to April 30, 2019. Edry, extremely dry; Sdry, severely dry; Mdry, moderately dry; Adry, abnormally dry; Ewet, extremely wet; Swet, severely wet; Mwet, moderately wet; Awet, abnormally wet.

processes (e.g., a few days long). At the same time, DEDI can be smoothed using different time windows, such as pentad, weekly, ten-day, monthly, seasonal, and annual windows, to meet the needs of users for drought analysis and monitoring at various timescales. Moreover, previous studies have demonstrated that DEDI has unique advantages in drought monitoring at different timescales. For example, Zhang et al. (2019) showed that the evapotranspiration difference index at a monthly timescale has a closer relationship with soil moisture and leaf area index than SPI, SPEI, or scPDSI, and can better describe the response of ecosystems to drought evolution. This study further verified the potential application of the index for drought monitoring using a daily timescale. Therefore, DEDI can not only monitor short-term (e.g., daily) droughts in real-time, but can also reflect the abnormal climate conditions of long-term water shortages (e.g., monthly and yearly timescales). DEDI can be used for meteorological drought monitoring and the assessment of water deficit impacts on agriculture and water resources.

4.2 Uncertainties in DEDI

The data quality of the variables used in the calculation of DEDI inevitably lends uncertainty to its evaluation. Because of the lack of long-term observational AET data and the sparse and uneven distribution of regular meteorological observation stations that can be used to calculate evapotranspiration, this study adopted the ERA5 reanalysis, newly developed by the European Center for Medium-Range Weather Forecasts, to calculate DEDI. ERA5 is a replacement for ERA-Interim data; however, although ERA5 uses higher-quality near-surface meteorological data to better

https://engine.scichina.com/doi/10.1007/s11430-021-9822-y

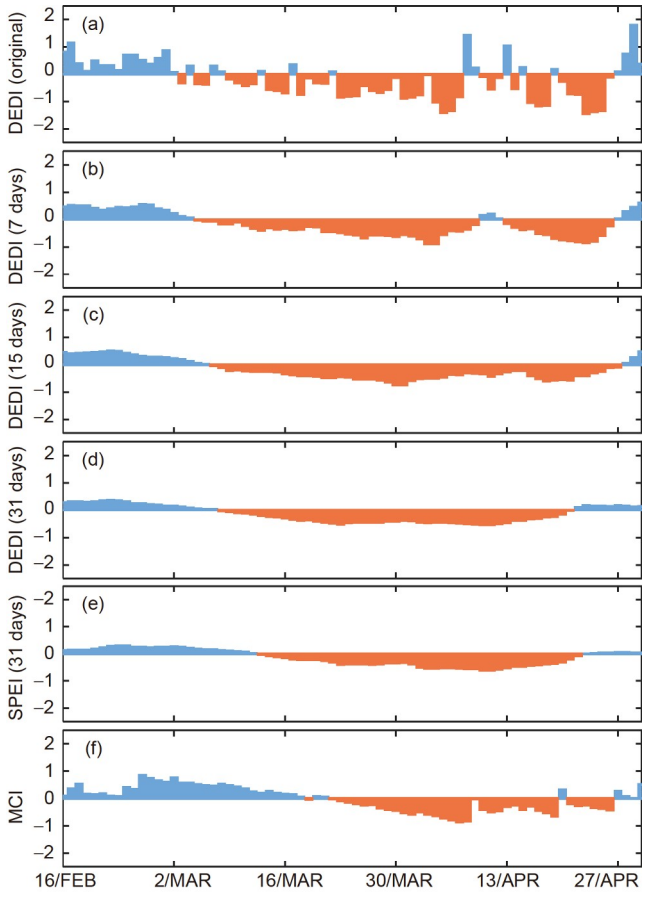

Figure 13 Daily evolutions of (a) the original DEDI values, (b)–(d) DEDI values after being smoothed over 7, 15, and 31 days, (e) the 31-day smoothed SPEI values, and (f) MCI, averaged over a typical arid region of northeast China including both Gansu Province and the Ningxia Hui Autonomous Region from February 16 to April 30, 2019.

characterize surface processes and surface heat budgets, it still has some uncertainties, for example, in data assimilation and assimilation technology. Its accuracy and applicability require further targeted evaluations, particularly in areas with complex terrain (Lucht et al., 2002; Martens et al., 2020). In addition, the highest spatial resolution of ERA5 data at present is 0.25°. Thus, the application of DEDI to reflect local dry and wet conditions at a finer scale still requires support from higher resolution data. In the coming years, with denser *in-situ* data (Granger, 1989; Allen et al., 1998; Qiu et al., 2003), more accurate remote sensing evapotranspiration methods (Zhang et al., 2010, 2016), and more realistic simulations of land surface models and surface water conditions (Chen et al., 1996, 2018), the calculation and study of DEDI will become more convenient and reliable.

At present, there is no perfect drought index that can be applied to all drought research objects and problems. For example, Heim Jr. (2002) pointed out that the Palmer index, a milestone in the history of developing drought indices, was originally designed to deal with droughts in semi-arid climate zones, and it has greater uncertainty under other climatic conditions. Yang et al. (2017) evaluated the performance of seven drought indices commonly used in recent years in China, including SPI, SPEI, and scPDSI. They showed that the regional applicability of each index is greatly affected by its own definition and by climate change. DEDI represents the difference between AET and PET; PET is mainly limited by energy under humid conditions and by available moisture under arid conditions, while PET is always primarily controlled by energy (Budyko, 1948). Because both AET and PET are mainly controlled by energy in humid and semi-humid regions, their differences are small, meaning that DEDI can show relatively large bias in these regions. Therefore, DEDI may be more suitable for arid and semi-arid regions, but further evaluation and verification are needed.

5. Conclusions

In this study, DEDI was constructed based on daily AET and PET using high-resolution ERA5 reanalysis data. The ability of DEDI to identify the drought signals of intense drought events and to characterize the drought evolution process was systematically assessed. Four drought events with different intensities that occurred in the southwest, north, northeast, and eastern northwest regions of China in the spring and summer 2019 were chosen to compare DEDI with the operational drought index of the Chinese National Climate Center, MCI, and a commonly used meteorological drought index, SPEI. The main conclusions are as follows:

(1) DEDI accurately detected the occurrence and evolution of the extreme drought events that occurred in the Yunnan Province, southwest China, in 2019. DEDI indicated that this extreme drought event started in late March and reached its peak in May. The drought eased slightly after the beginning of the rainy season in the southwest in June, and most areas reached a normal or humid state in July. A relatively strong drought process, but with a short duration, appeared again in August, and the region then returned to normal in early September. SPEI presented similar drought characteristics (in terms of timing and drought intensity evolution) to DEDI. In contrast, the drought process monitored by MCI, from development, to peak, to alleviation, lagged somewhat. MCI accumulates dry and wet conditions over the previous five months, meaning that it could easily miss the short-term characteristics of drought evolution. Therefore, the MCI did not capture the second drought intensity peak that occurred in August. The analysis of the heaviest drought, which occurred in the typical arid region in central and western Yunnan Province, showed that the drought intensity and extreme drought coverage percentage identified by DEDI in August was comparable to the first drought process, in-

https://engine.scichina.com/doi/10.1007/s11430-021-9822-y

dicating the relevant impacts of the second drought process, despite its short duration. Moreover, the analysis of climatic DEDI from 1979 to 2019 also revealed the rare and extreme nature of this drought process.

(2) To verify the regional applicability of DEDI, the index was further applied to monitor strong drought events that occurred in north, northeast, and eastern northwest China in 2019. In north China, DEDI reproduced the drought process that began to develop in early March, reaching a peak in late March, and decreasing in both intensity and extent from April onwards. In northeast China, DEDI detected that the drought developed in April and rapidly reached its peak intensity from early May to mid-May, particularly in Jilin Province, where the extreme drought lasted about a week. The drought was then relieved from mid- to late May owing to its short duration and the rapid arrival of precipitation. In eastern northeast China, DEDI monitored the rapid development of drought, starting from the northern Gansu Province and moving southeast in early March. In mid-late March to mid-late April, almost all of the Ningxia Hui Autonomous Region and Gansu Province were in a state of moderate drought or worse. The drought was finally relieved in late April. Although the intensities and durations of these three drought events were not as strong as those of the drought in southwest China, DEDI still showed reasonable and accurate monitoring abilities.

(3) The application of DEDI in drought monitoring has both advantages and uncertainties. By integrating the effects of temperature and precipitation, DEDI can more sensitively reflect the amount of surface water deficit. It also considers land surface conditions such as vegetation cover and soil. Therefore, DEDI can be used as an indicator for meteorological drought monitoring and early warning systems, and has the potential for application in agricultural drought monitoring. Compared with MCI, DEDI can detect discrepancies in water deficit on different days, which can provide necessary details for drought monitoring. The quality of the available evapotranspiration data contributes most to the uncertainty of DEDI. Nevertheless, in the coming years, improvements in observations, reanalysis data, land surface models, and remote sensing retrieval methods for evapotranspiration should help to reduce this uncertainty. Moreover, the applicability of DEDI in other regions requires further verification.

Acknowledgements *This work was supported by the National Key R&D Program of China (Grant No. 2018YFC1508701).*

References

Allen R G, Pereira L S, Raes D, Smith M. 1998. Crop Evapotranspiration—Guidelines for computing crop water requirements—FAO Irrigation and Drainage Paper 56. Technical Report. Rome, 56: 15–64

Anderson M C, Hain C, Wardlow B, Pimstein A, Mecikalski J R, Kustas W P. 2011. Evaluation of drought indices based on thermal remote sensing of evapotranspiration over the continental United States. J Clim, 24: 2025–2044

Budyko M I. 1948. Evaporation under Natural Conditions. Leningrad: Gidrometeorologicheskoe Izdatel'stvo. 136

Calviño P A, Andrade F H, Sadras V O. 2003. Maize yield as affected by water availability, soil depth, and crop management. Agron J, 95: 275–281

Chen F, Mitchell K, Schaake J, Xue Y K, Pan H L, Koren V, Duan Q Y, Ek M, Betts A. 1996. Modeling of land surface evaporation by four schemes and comparison with FIFE observations. J Geophys Res, 101: 7251–7268

Chen F, Xu X, Barlage M, Rasmussen R, Shen S, Miao S, Zhou G. 2018. Memory of irrigation effects on hydroclimate and its modeling challenge. Environ Res Lett, 13: 064009

Couturier S, Taylor D, Siegert F, Hoffmann A, Bao M Q. 2001. ERS SAR backscatter: A potential real-time indicator of the proneness of modified rainforests to fire. Remote Sens Environ, 76: 410–417

Dai A. 2011a. Characteristics and trends in various forms of the Palmer Drought Severity Index during 1900–2008. J Geophys Res, 116: D12115

Dai A. 2011b. Drought under global warming: A review. WIREs Clim Change, 2: 45–65

Dai A. 2013. Increasing drought under global warming in observations and models. Nat Clim Change, 3: 52–58

Ding T, Gao H. 2020. The record-breaking extreme drought in Yunnan Province, Southwest China during Spring-early Summer of 2019 and possible causes. J Meteorol Res, 34: 997–1012

General Administration of Quality Supervision, Standardization Administration. 2017. GB/T 20481-2017 Grades of Meteorological Drought (in Chinese). Beijing: Standards Press of China

Granger R J. 1989. A complementary relationship approach for evaporation from nonsaturated surfaces. J Hydrol, 111: 31–38

Guttman N B. 1999. Accepting the standardized precipitation index: A calculation algorithm. JAWRA J Am Water Resour Assoc, 35: 311–322

Han L Y, Zhang Q, Jia J Y, Wang Y H, Huang T. 2019. Drought severity, frequency, duration and regional differences in China (in Chinese). J Desert Res, 39: 1–10

Hao Z, AghaKouchak A, Phillips T J. 2013. Changes in concurrent monthly precipitation and temperature extremes. Environ Res Lett, 8: 034014

Heim Jr. R R. 2002. A review of twentieth-century drought indices used in the United States. Bull Amer Meteorol Soc, 83: 1149–1166

Hersbach H, Bell B, Berrisford P, Hirahara S, Horányi A, Muñoz-Sabater J, Nicolas J, Peubey C, Radu R, Schepers D, Simmons A, Soci C, Abdalla S, Abellan X, Balsamo G, Bechtold P, Biavati G, Bidlot J, Bonavita M, Chiara G, Dahlgren P, Dee D, Diamantakis M, Dragani R, Flemming J, Forbes R, Fuentes M, Geer A, Haimberger L, Healy S, Hogan R J, Hólm E, Janisková M, Keeley S, Laloyaux P, Lopez P, Lupu C, Radnoti G, Rosnay P, Rozum I, Vamborg F, Villaume S, Thépaut J N. 2020. The ERA5 global reanalysis. QJR Meteorol Soc, 146: 1999–2049

Hobbins M T, Ramírez J A, Brown T C. 2004. Trends in pan evaporation and actual evapotranspiration across the conterminous U.S.: Paradoxical or complementary? Geophys Res Lett, 31: L13503

Huang J P, Zhang G L, Yu H P, Wang S S, Guan X D, Ren Y. 2020. Characteristics of climate change in the Yellow River basin during recent 40 years (in Chinese). J Hydraul Eng, 51: 1048–1058

Huang R H, Cai R S, Chen J L, Zhou L T. 2006. Interdecaldal variations of drought and flooding disasters in China and their association with the East Asian climate system (in Chinese). Chin J Atmos Sci, 30: 730–743

Huang R H, Liu Y, Wang L, Wang L. 2012. Analyses of the causes of severe drought occurring in southwest China from the Fall of 2009 to the Spring of 2010 (in Chinese). Chin J Atmos Sci, 36: 443–457

Huang R H, Zhou L T. 2002. Research on the characteristics, formation mechanism and prediction of severe climatic disasters in China (in Chinese). J Nat Disasters, 11: 1–9

Hunt E D, Svoboda M, Wardlow B, Hubbard K, Hayes M, Arkebauer T. 2014. Monitoring the effects of rapid onset of drought on non-irrigated

https://engine.scichina.com/doi/10.1007/s11430-021-9822-y

maize with agronomic data and climate-based drought indices. Agric For Meteorol, 191: 1–11
Huo Z G, Zheng J P, Xu X D, Bai Y M, Wen M, Wang C Y. 2000. Simulation experiment of possible effects of various arid periods in spring on winter wheat in north China (in Chinese). Resour Sci, 22: 72–76
Jia Y Q, Zhang B. 2018. Spatial-temporal variability characteristics of extreme drought events based on daily SPEI in the southwest China in recent 55 years (in Chinese). Sci Geogr Sin, 38: 474–483
Li J, Wang Z L, Wu X S, Zscheischler J, Guo S L, Chen X H. 2021. A standardized index for assessing sub-monthly compound dry and hot conditions with application in China. Hydrol Earth Syst Sci, 25: 1587–1601
Liao Y M, Zhang C J. 2017. Spatio-temporal distribution characteristics and disaster change of drought in China based on meteorological drought composite index (in Chinese). Meteor Mon, 43: 1402–1409
Liu H Z, He L F. 2019. Analysis of the June 2019 atmospheric circulation and weather (in Chinese). Meteor Mon, 45: 1335–1340
Lu H J, Mo X G, Meng D J, Liu S X. 2015. Analyzing spatiotemporal patterns of meteorological drought and its responses to climate change across northeast China (in Chinese). Sci Geogr Sin, 35: 1051–1059
Lucht W, Prentice I C, Myneni R B, Sitch S, Friedlingstein P, Cramer W, Bousquet P, Buermann W, Smith B. 2002. Climatic control of the high-latitude vegetation greening trend and Pinatubo effect. Science, 296: 1687–1689
Ma J H, Liu Y, Yang X G, Wang W F, Xue C Y, Zhang X Y. 2010. Characteristics of climate resources under global climate change in the North China Plain (in Chinese). Acta Ecol Sin, 30: 3818–3827
Ma Z G. 2005. Dry/wet variation and its relationship with regional warming in arid-regions of norther China (in Chinese). Chin J Geophys, 48: 1011–1018
Ma Z G, Fu C B. 2001. Trend of surface humid index in the arid area of northern China (in Chinese). Acta Meteorol Sin, 59: 737–746
Ma Z, Fu C. 2006. Some evidence of drying trend over northern China from 1951 to 2004. Chin Sci Bull, 51: 2913–2925
Ma Z G, Fu C B. 2007. Global aridification in the second half of the 20th century and its relationship to large-scale climate background. Sci China Ser D-Earth Sci, 50: 776–788
Ma Z G, Shao L J. 2006. Relationship between dry/wet variation and the pacific decade oscillation (PDO) in northern China during the last 100 years (in Chinese). Chin J Atmos Sci, 30: 464–474
Mao F, Sun H, Yang H L. 2011. Research progress in dry/wet climate zoning (in Chinese). Progr Geoger, 30: 17–26
Martens B, Schumacher D L, Wouters H, Muñoz-Sabater J, Verhoest N E C, Miralles D G. 2020. Evaluating the land-surface energy partitioning in ERA5. Geosci Model Dev, 13: 4159–4181
McEvoy D J, Huntington J L, Hobbins M T, Wood A, Morton C, Anderson M, Hain C. 2016. The evaporative demand drought index. Part II: CONUS-wide assessment against common drought indicators. J Hydrometeorol, 17: 1763–1779
McKee T B, Doesken N J, Kleist J. 1993. The relationship of drought frequency and duration to time scales. In: 8th Conference on Applied Climatology. Anaheim. 179–184
McRoberts D B, Nielsen-Gammon J W. 2012. The use of a high-resolution standardized precipitation index for drought monitoring and assessment. J Appl Meteor Climatol, 51: 68–83
Meyer S J, Hubbard K G, Wilhite D A. 1993. A crop-specific drought index for corn: I. Model development and validation. Agron J, 85: 388–395
Qiu X F, Zeng Y, Miao Q L, Yu Q. 2004. Estimation of annual actual evapotranspiration from nonsaturated land surfaces with conventional meteorological data. Sci China Ser D, 47: 239–246
Ren L, Zhou T, Zhang W. 2020. Attribution of the record-breaking heat event over Northeast Asia in summer 2018: The role of circulation. Environ Res Lett, 15: 054018
Scheff J, Frierson D M W. 2014. Scaling potential evapotranspiration with greenhouse warming. J Clim, 27: 1539–1558
State Scientific and Technological Commission. 1990. Climate (in Chinese). Beijing: Scientific and Technical Documentation Press. 18
Su B D, Sun H M, Li X C, Li Z J, Zhang J P, Wang Y J, Huang J L, Gao M N, Jiang T, Si L L. 2020. Impact of climate change on terrestrial water cycle in China (in Chinese). Trans Atmos Sci, 43: 1096–1105
Sun G H, Hu Z Y, Ma Y M, Xie Z P, Yang S, Wang J M. 2020. Analysis of local land-atmosphere coupling in rainy season over a typical underlying surface in Tibetan Plateau based on field measurements and ERA5. Atmos Res, 243: 105025
Svoboda M, Lecomte D, Hayes M, Heim R, Gleason K, Angel J, Rippey B, Tinker R, Palecki M, Stooksbury D, Miskus D, Stephens S. 2002. The drought monitor. Bull Amer Meteorol Soc, 83: 1181–1190
Tu G, Liu B, Wang S Y. 2012. Spatial-temporal characteristics of surface dry/wet status in northeast China by NCAR/CLM3.5 (in Chinese). Sci Geogr Sin, 32: 746–751
Vicente-Serrano S M, Beguería S, López-Moreno J I. 2010. A multiscalar drought index sensitive to global warming: The standardized precipitation evapotranspiration index. J Clim, 23: 1696–1718
Vicente-Serrano S M, Beguería S, Lorenzo-Lacruz J, Camarero J J, López-Moreno J I, Azorin-Molina C, Revuelto J, Morán-Tejeda E, Sanchez-Lorenzo A. 2012. Performance of drought indices for ecological, agricultural, and hydrological applications. Earth Interactions, 16: 1–27
Vicente-Serrano S M, Gouveia C, Camarero J J, Beguería S, Trigo R, López-Moreno J I, Azorín-Molina C, Pasho E, Lorenzo-Lacruz J, Revuelto J, Morán-Tejeda E, Sanchez-Lorenzo A. 2013. Response of vegetation to drought time-scales across global land biomes. Proc Natl Acad Sci USA, 110: 52–57
Vicente-Serrano S M, Van der Schrier G, Beguería S, Azorin-Molina C, Lopez-Moreno J I. 2015. Contribution of precipitation and reference evapotranspiration to drought indices under different climates. J Hydrol, 526: 42–54
Wang H, Chen Y, Pan Y, Chen Z, Ren Z. 2019. Assessment of candidate distributions for SPI/SPEI and sensitivity of drought to climatic variables in China. Int J Climatol, 39: 4392–4412
Wang L, Chen W. 2014. Applicability analysis of standardized precipitation evapotranspiration index in drought monitoring in China (in Chinese). Plateau Meteorol, 33: 423–431
Wang L Y, Yuan X. 2018. Two types of flash drought and their connections with seasonal drought. Adv Atmos Sci, 35: 1478–1490
Wang S P, Wang J S, Zhang Q, Li Y P, Wang Z L. 2015. Applicability Evaluation of drought indices in monthly scale drought monitoring in southwestern and southern China (in Chinese). Plateau Meteorol, 34: 1616–1624
Wei F Y, Zhang T. 2009. Frequency distribution of drought intensity in Northeast China and relevant circulation background (in Chinese). J Nat Disasters, 18: 1–7
Wells N, Goddard S, Hayes M J. 2004. A self-calibrating palmer drought severity index. J Clim, 17: 2335–2351
Xu G Y, Yang X Q, Sun X G. 2005. Interdecadal and interannual variation characteristics of rainfall in north china and its relation with the northern hemisphere atmospheric circulations (in Chinese). Chin J Geophys, 48: 511–518
Yang Q, Li M X, Zheng Z Y, Ma Z G. 2017. Regional applicability of seven meteorological drought indices in China. Sci China Earth Sci, 60: 745–760
Yao H. 1992. Division and chances of precipitation in the northwest of China in recent several ten years (in Chinese). Arid Land Geoger, 15: 27–33
Yuan X, Wang Y M, Zhang M, Wang L Y. 2020. A few thoughts on the study of flash drought (in Chinese). Trans Atmos Sci, 43: 1086–1095
Zhang K, Kimball J S, Nemani R R, Running S W. 2010. A continuous satellite-derived global record of land surface evapotranspiration from 1983 to 2006. Water Resour Res, 46: W09522
Zhang K, Kimball J S, Running S W. 2016. A review of remote sensing based actual evapotranspiration estimation. WIREs Water, 3: 834–853
Zhang Q, Yao Y B, Li Y H, Huang J P, Ma Z G, Wang Z L, Wang S P, Wang Y, Zhang Y. 2020. Progress and prospect on the study of causes

https://engine.scichina.com/doi/10.1007/s11430-021-9822-y

and variation regularity of droughts in China (in Chinese). Acta Meteorol Sin, 78: 500–521
Zhang Q, Zhao Y D, Zhang C J, Li Y H, Sun G W, Gao Q Z. 2008. Issues about hydrological cycle and water resource in arid region of northwest China (in Chinese). Arid Meteorol, 26: 1–8
Zhang Q Y, Wei J, Tao S Y. 2003. The decadal and interannual variations of drought in the northern China and association with the circulations (in Chinese). Clim Environ Res, 8: 307–318
Zhang S Y. 2008. Arid Meteorology (in Chinese). Beijing: China Meteorological Press. 23
Zhang X, Li M, Ma Z, Yang Q, Lv M, Clark R. 2019. Assessment of an evapotranspiration deficit drought index in relation to impacts on ecosystems. Adv Atmos Sci, 36: 1273–1287
Zou X K, Ren G Y, Zhang Q. 2010. Droughts variations in China based on a compound index of meteorological drought (in Chinese). Clim Environ Res, 15: 371–378

(Responsible editor: Jianping HUANG)

https://engine.scichina.com/doi/10.1007/s11430-021-9822-y